Relating Photoelectrochemistry and Wettability of Sputtered Cu- and N-doped TiO_2 Thin Films *via* an Integrated Approach

Corrado Garlisi,[1] Chia-Yun Lai,[2] Leslie George,[3] Matteo Chiesa,[2,4]* Giovanni Palmisano[1,]*

[1] Department of Chemical Engineering, Khalifa University of Science and Technology, Masdar Institute, Masdar City, PO BOX 54224, Abu Dhabi, United Arab Emirates. Email: gpalmisano@masdar.ac.ae
[2] Laboratory for Energy and Nano Science, Khalifa University of Science and Technology, Masdar Institute, Masdar City, P.O Box 54224, Abu Dhabi, United Arab Emirates. Email: mchiesa@masdar.ac.ae
[3] Department of Research Laboratories, Khalifa University of Science and Technology, Masdar Institute, Masdar City, PO BOX 54224, Abu Dhabi, United Arab Emirates
[4] Arctic Center for Sustainable Energy – ARC, Department of Physics and Technology, University of Tromsø, Norway

Abstract

We present here an integrated study of the photoelectrochemical and hydrophilic properties of sputtered TiO_2 thin films, enhanced by means of nitrogen (N)- and copper (Cu)- doping. We investigated the effect that doping has on both photoelectrochemical efficiency and surface properties by employing a variety of techniques spanning from impedance electrochemical impedance spectroscopy (EIS), static contact angle and AFM force spectroscopy before and after UV irradiation, through a comprehensive approach able to connect photelectrochemical and hydrophilic performance. Namely, Cu doping was observed to worsen TiO_2 photoelectrochemical efficiency, unlike N-doping that instead improved it, while both doping enhanced the surface chemistry. Both doping resulted in anodic shift of the flat band potential and in an increase in the donor density with the occurrence of surface defects beneficial for the separation of charge carriers in N-TiO_2 on one side, and more recombination centers in Cu-TiO_2 on the other. On the other hand, macroscopic wettability characterization indicated that Cu-TiO_2 and N-TiO_2 had a much lower contact angle than TiO_2 (SCA≈ 20° and 10° for Cu-doped and N-doped films, respectively, as compared to 50° in the bare film) and became superhydrophilic after UV irradiation; AFM corroborated contact angle data, pointing out that the enhanced hydrophilicity in doped films can be ascribed to an alteration in the surface chemistry because of a greater number of surface defects, such as oxygen vacancies, acting as binding sites for water molecules.

1. Introduction

The continuing and increasing attention on solar-driven technologies has encouraged intense research activities on innovative structures and semiconducting materials able to face the growing global energy demand and concern for climate change. Titanium oxide (TiO_2)-based materials still remain among the preferred choice for applications in energy and environmental areas such as photocatalysis,[1-2] self-cleaning coatings of solar cells [3-4] and photoelectrodes in photoelectrochemcal (PEC) cells.[5-7] In most of these applications, TiO_2 is used in form of thin films and it is required to provide an enhanced performance in terms of photoelectrochemical and wettability properties. The first feature implies good light absorption, efficient charge carrier transport, fast charge transfer kinetics, etc., all these aspects being fundamental for the direct generation of solar fuels and photo-degradation of pollutants; on the other hand, the second feature implies a "water loving" surface on which the water can spread evenly to form a thin film and wash off the dirt particles while flowing, being crucial to keep the coated object clean and virtually dirt-free. Most of the times hydrophilicity, such as in TiO_2, is boosted by UV-vis irradiation which increases in the number of surface hydroxyl groups, resulting in the alteration of the interfacial energy between the solid surface and the liquid.[8] On the other hand, photo-electrochemical water splitting, despite being a promising pathway to produce hydrogen from water using sunlight, yields low energy conversion efficiency, something that hinders economically scalable solutions. Arguably, the tunable photochemical characteristics of TiO_2 in combination with the good affinity for water justify the effort presented in this paper.

One of the main approaches used to improve the performance of TiO_2-based materials is doping either with metal or non-metal elements. For this purpose, copper (Cu) and nitrogen (N) can be effectively introduced into TiO_2 crystal lattice, generally as substitutional species, replacing titanium and oxygen, respectively. These elements normally improve charge separation as well as absorption and reactivity in the visible region.[9-10] Most of the times, these properties are greatly affected by the introduction of point defects as a result of the doping which leads to oxygen vacancies and impurities states, having for example a significant impact on the wettability in the dark and on the way in which the semiconductor responds to UV-light becoming highly hydrophilic. Conversely, doping can also lead to an adverse performance depending on the nature of the doping element, its concentration, oxidation state and how it is incorporated into TiO_2 crystal lattice (i.e. substitutionally or interstitially).[11-12] Indeed, the element may end up, following atomic

rearrangements and surface reconstruction, introducing trap states acting as recombination centers for the generated photocarriers, with resultant disadvantages for TiO_2 efficiency.

In this context, it is therefore clear that a deeper understanding of the doping effects is desirable in order to improve the performance of the current technologies making use of TiO_2. To this aim, we adopt a novel approach to correlate photoelectrochemical behavior with wettability properties of N-TiO_2 and Cu-TiO_2 thin films, pointing out how the two types of doping alter the material performance as compared to bare TiO_2 and the response to UV/Vis stimulation. While, on the one hand, electrochemical behavior was assessed by anodic photocurrent response and impedance spectroscopy, on the other, wettability was explored by an integrated nano- and macroscale approach, which was already used in one of our previous work to study the changes in hydrophilicity of pure TiO_2 films following annealing treatment.[13] That study, which combined contact angle and AFM measurements, showed how AFM provides a versatile and convenient tool to gain deeper physical insight into the nanoscale mechanisms that determine the wetting properties of TiO_2, allowing the direct investigation of surface chemistry modification independently of morphological effects. Wettability, however, is not the only property being affected by surface chemistry, but it is well established that, for oxide semiconductor materials, this also affects fundamental transfer charge processes in photocatalytic reactions. Indeed, many of the aforementioned defects are located at the semiconductor surface and play a crucial role in the final photoelectrochemical efficiency of a number of TiO_2-based devices. For example, surface oxygen vacancies can act as charge carrier traps as well as adsorption sites where the charge transfer to adsorbed species prevent the surface charge recombination.[14] The double approach proposed in this work – electrochemical and wettability measurements – is able to provide an insight into how metal and non-metal doping modify photoelectrochemical and hydrophilic properties of TiO_2, and how these two aspects, both crucial for the design of increasingly advanced solar-driven technologies, can be linked to each other and, in turn, to the surface chemistry.

2. Experimental section

2.1 Sample preparation and structural characterization

TiO_2-based thin films were deposited on soda-lime glass substrates (25x75 mm, Sigma-Aldrich) using radiofrequency (RF) magnetron sputtering (AJA ATC Orion Series). Prior to deposition, the

substrates were cleaned in ultrasonic bath during 10 min in acetone and 10 min in isopropanol successively. Samples were labelled as X-TiO_2 were X is the doping element.

TiO_2, Cu-TiO_2 and N-TiO_2 films were obtained while depositing with TiO_2 (99.9% pure), TiO_2:Cu (atomic ratio TiO_2:Cu = 98.5:1.5) and TiO_2:N (atomic ratio TiO_2:N = 98.5:1.5) targets, respectively. The base pressure for all deposition was ~ 4 to 6 $x10^{-7}$ Torr.

Prior to all the depositions, targets were pre-sputtered during 10 min to remove any surface contamination. Argon was used as the sputtering gas for deposition with a constant pressure of 10 mTorr and a flow rate of 30 sccm (standard cubic centimeters per minute). The RF power of the cathode was 250 W and film were deposited at room temperature. The distance between the target and the substrate holder was fixed at 14 cm. The total film thickness was around 100 nm and Stylus profilometer (Veeco Dektak 150) was used to measure the film thickness. After deposition, films were annealed in air applying the following steps: heating up to 475°C (ramp rate of 10°C/min), 5 min at 475°C, heating up to 500°C (ramp rate of 2.5°C/min), 4 hours at 500°C, then they were left cooling down slowly keeping the furnace closed to avoid temperature shocks.

The crystalline structure of the as prepared catalysis was studied with an X-Ray diffraction machine (Empyrean from PANalytical). Samples were irradiated with X-rays generated by a Cu-K_α source (radiation wavelength of 1.54 Å). Experiments were done in the 2θ configuration and the diffracted signal was acquired within a scan range of 10-90° with a scan step-size of 0.0167°.

2.2 Electrochemical characterization

Photoelectrochemical measurements were carried out using a Metrohm Autolab PGSTAT302N Potentiostat in a standard three electrode cell with the sample deposited on FTO as working electrode, platinum electrode as counter electrode and Ag/AgCl electrode as reference. The electrolyte solution was 0.5 M Na_2SO_4 (pH 5.6). Linear sweep voltammetry was performed at a scan rate of 20 mV s^{-1} in the dark and under UV/Vis illumination. Photocurrent transient were recorded at a potential of 0.9 V vs. NHE. Electrochemical impedance spectroscopy (EIS) was performed in dark and under UV/Vis illumination in the frequency range of 0.1 Hz – 10 kHz with an applied potential of 0.9 V vs. NHE. Mott-Schottky experiments were conducted with potential step of 50 mV at a constant frequency of 10 kHz. For experiments performed under UV/Vis light, a 50 W LED source with an emission centred at 385 nm was used. The average values of the

radiation reaching the sample surface, measured with a DeltaOhm 9721 radiometer and the matching probes, were 52.8 and 41.6 W m^{-2} in the 315–400 and 450–950 nm ranges.

2.3 Contact angle measurements

Water static contact angle (SCA) was measured by a Kruss Easy Drop Contact Angle analysis machine and the standard software supplied by Krüss was used for the evaluation of the data. All the samples were cleaned in acetone and then in ethanol in two successive 5-minute steps and finally dried under Argon flow. Samples were then heated at 50°C for 30 min to remove possible volatile organic residues. SCA was measured using 5 μL droplets and five consecutive measurements were performed on each sample to report a reliable average value. The time evolution of the SCA under UV/Vis light was studied by irradiating samples with the same UV/Vis light used during the photoelectrochemical characterization.

2.4 Atomic force microscope force spectroscopy measurements

Atomic force microscope (AFM) force spectroscopy measurements were carried out with Cypher AFM from Asylum Research and standard OLYMPUS cantilevers (AC160TS) with $k \approx 20$ N/m, $Q \approx 300$, and $f_0 \approx 250$ kHz were used. The AFM was operated in amplitude modulation mode for obtaining force profiles. To reconstruct the force profile, we employed Sader−Jarvis−Katan formalism.[15-16] The detailed procedure his is described elsewhere.[17-18] Briefly, we recorded the observables amplitude A and phase lag ϕ as a function of tip−sample separation distance d, *i.e*. APD curves. Free cantilever oscillation amplitudes of 30 nm were used to record the APD curves to avoid bistability. Furthermore, as we know that the tip radius R has a great effect on the reconstructed force, we constantly monitored R *in situ* with critical amplitude method[19] to ensure that there was no change in R during a set of experiment. A total of 150 APD curves were collected on each sample and respective state, *i.e*. before and after UV/Vis irradiation, for statistical analysis. The measurements after UV exposure were carried out after 30 min of continuous irradiation by the same UV/Vis light used for photoelectrochemical characterization and contact angle analysis.

3. Results and discussion

All the films were crystalline, anatase being the only detected phase (Fig. S1). The photoelectrochemical properties of the thin films were studied under linear sweep voltammetry

conditions in the dark and under UV/Vis irradiation and data are presented in Figure 1a. The rise of the photocurrent intensity at less negative potentials follows a larger potential drop within the space charge region in n-type semiconductors. Indeed, current densities *J* of the three samples increased with increasing anodic bias under UV//Vis irradiation. The photocurrent density of N-TiO_2 increased faster than the other two samples reaching 77 μA cm^{-2} at 1.2 V (vs. NHE) as opposed to 40 and 32 μA cm^{-2}, which were found for pristine TiO_2 and Cu-TiO_2, respectively. The photoconversion efficiency η, related to the conversion of light to chemical energy, can be computed from the *J-V* data using the following equation[20-21]:

$$\eta = \frac{J\left(1.23 - E_{app}\right)}{I_0} \quad (1)$$

Where E_{app} is the applied potential (vs. NHE) and I_0 is the power density of the incident light (9.4 mW/cm^2). As shown in the inset of Figure 1a, N-TiO_2 achieved the maximum efficiency of 0.29% at 0.64 V (vs. NHE), whereas TiO_2 and Cu-TiO_2 reached a maximum efficiency of 0.18% and 0.15%, both at 0.54 V (vs. NHE). Transient current response measurements, which are shown in in Figure 1b, are consistent with linear sweep voltammetry and photoconversion efficiency. They exhibit an anodic stationary photocurrent, appearing promptly upon switching-on the light with the presence of spikes of the same sign and then decreasing sharply to finally reach a steady state value. The steady state photocurrent density of the N-TiO_2 (55 μA cm^{-2}) was ca. 1.6 and 1.9 times as high as compared to bare TiO_2 (35 μA cm^{-2}) and Cu-TiO_2 (29 μA cm^{-2}). The higher photocurrent density of N-TiO_2 gives evidence of an enhanced separation of the photoexcited electron−hole pairs and a minor concentration of trap states as will be discussed in the following.[22-23]

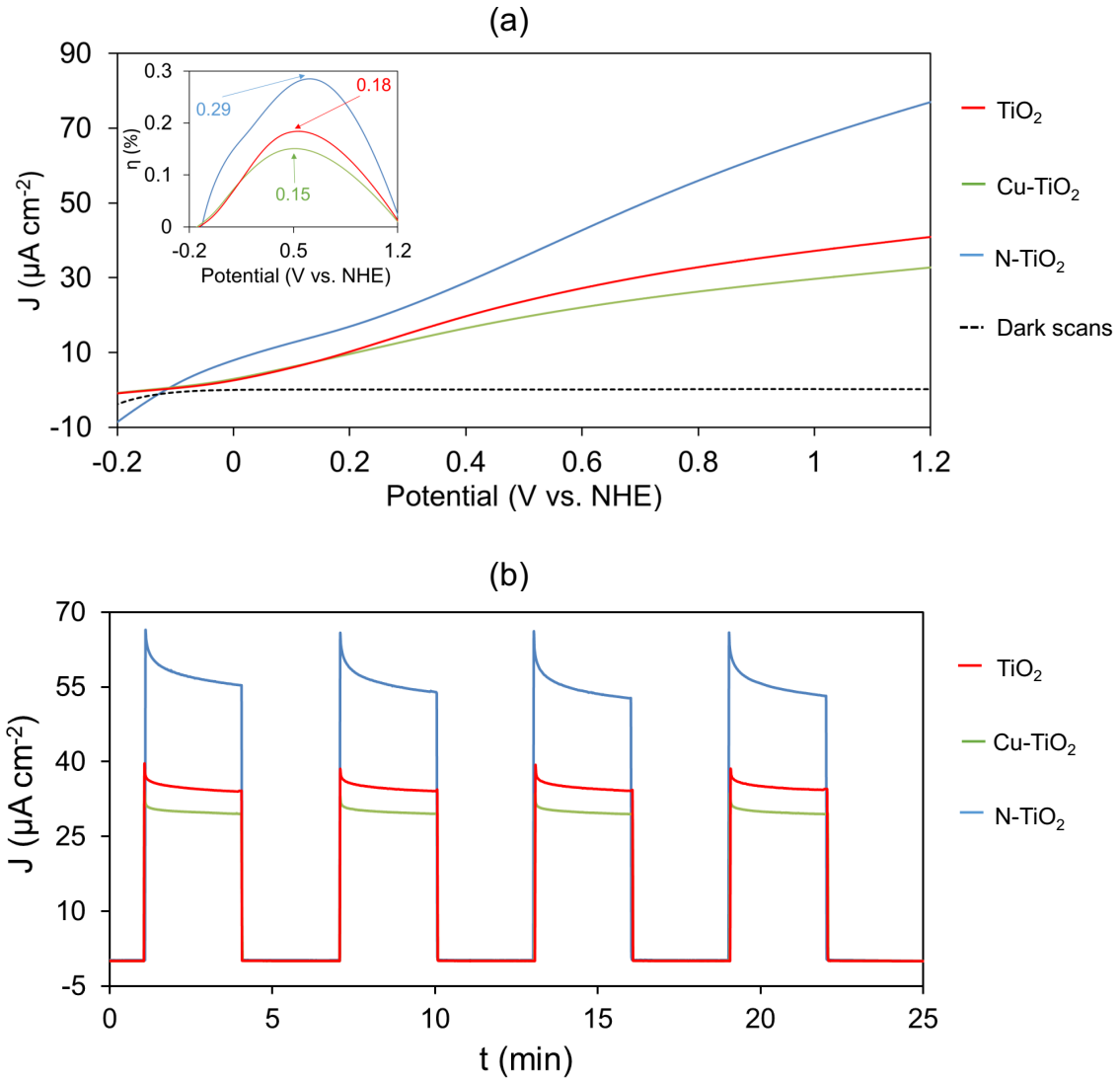

Figure 1. **(a)** Linear sweep voltammograms of the tree samples; the inset shows the photoconversion efficiency. **(b)** Photocurrent transient generated at 0.9 V vs. NHE under UV/Vis irradiation.

EIS measurements were performed to investigate kinetics of charge transfer at the solid-liquid interface and data were fitted to the equivalent model for a double capacitor illustrated in Fig.2a, where R_s is the series resistance including FTO substrate, external contact resistance and electrolyte resistance; the high frequency response (100 Hz ÷ 10 KHz) is described by CPE_1 and R_1 which are the bulk semiconductor capacitance and resistance; the low frequency response is assigned to CPE_2 and R_2 accounting for the Helmholtz capacitance and semiconductor/electrolyte charge transfer resistance, respectively.[24-25] In dark conditions, as shown in the Nyquist plot of the inset in Fig. 2a, the semicircle is too large to be fully observed due to the high resistance of the semiconductor/electrolyte interface resulting in a minor charge transfer process in line with the

negligible dark current observed in Fig. 1. On the other hand, the resistance to charge transfer is much lower under UV/Vis irradiation due to the generated photocarriers, resulting in clearly distinguishable circular arcs for all the samples, where N-TiO_2 is the one with smaller radius. The values of R_1, R_2 and CPE_2 fitted by the equivalent circuit are shown in table 1. The resistance R_1 and R_2 of N-TiO_2 are significantly lower than that of the other two films, thus confirming the improved separation efficiency of photoinduced carriers and faster charge transfer at the film-liquid interface as compared to bare TiO_2 and Cu-TiO_2. The beneficial effect of the nitrogen doping can be also inferred by the values of the Helmholtz capacitance, which arises from the buildup of electrons in the TiO_2 film. Such capacitance designates the variation of electron density following a small change of the Fermi level, providing the total density of the free electrons in the semiconductor conduction band and localized electrons in trap states.[26] The lowest value of CPE_2 in N-TiO_2 is indicative of the fact that less photoinduced electrons are captured by empty trap states, thereby facilitating the electron transport to Pt counter electrode. As a consequence, the remaining holes do not recombine with electrons, but transfer to the electrode. On the other hand, copper doping negatively affects the kinetics of charge transfer as showed in Fig. 2a and values in Table 1, resulting in a slightly poorer performance as compared to bare TiO_2, indicating the emergence of trap states and recombination centers caused by this type of doping.

Mott-Schottky plots, obtained by electrochemical impedance measurements at a constant frequency of 10 kHz, are presented in Fig. 2b. Electronic properties of the three thin films were assessed in terms of the flat band potential (E_{FB}) and donor density (N_D) which can be obtained as the intercept with x-axis and from the slope of the linear part of the plot, which is positive in the case of n-type semiconductors. According to the Mott-Schottky equation,[27] the capacitance (C) of a semiconductor can be calculated as:

$$\frac{1}{C^2} = \frac{2}{\varepsilon_0 \varepsilon e N_D}\left(E - E_{FB} - \frac{kT}{e}\right) \quad (2)$$

where E is the applied potential, T the temperature (ca. 298 K), k the Boltzmann constant and ε_0 = 8.854×10^{-14} F cm^{-1}, $\varepsilon = 50$, $e = 1.602 \times 10^{-19}$ C are the vacuum permittivity, dielectric constant of anatase TiO_2 and electron charge, respectively. N_D can be thus derived through the equation:

$$N_D = \left(\frac{2}{\varepsilon_0 \varepsilon e}\right)\left(\frac{dE}{d\left(\frac{1}{C^2}\right)}\right) \quad (3)$$

E_{FB} and N_D values are reported in table 1. The flat band potential is indicative of the situation in which there is no accumulation of charge within the semiconductor, so that the energy bands do not undergo bending, and it corresponds to conduction band edge in compact n-type TiO_2 thin films like the ones studied in the present work.[27] Compared to the pure TiO_2 film, both Cu-TiO_2 and N-TiO_2 show a positive shift of E_{FB}, indicating a reduction in the bending of the band edges following the doping. The introduction of both metal and non-metal doping thus resulted in an anodic shift of the conduction band, which is more evident in Cu-TiO_2. The origin of this shift can be multifold. In general, the presence of a large number of surface states and oxygen vacancies in the semiconductor can favor a variation of the band position. In the present case, the main reason for such shift is the doping and thus the presence of copper and nitrogen (concentrations of ca. 0.5 at.%) in the form of Cu^+ and N^{3-}, with Cu^+ replacing lattice O^{2-} and N^{3-} replacing Ti^{4+}, as demonstrated by XPS analysis performed in our previous studies on the same materials.[28] It is believed that nitrogen doping affects anatase structure through the mixing of N 2p states with O 2p states, along with the boosting of oxygen vacancies, which results in donor states below the bottom of conduction bands.[29-31] On the other hand, since ionic radius of Cu^+ ion (90 Å) is not too different from Ti^{4+} ion (0.75 Å), Cu^+ can easily preplace Ti^{4+} in TiO_2 structure giving rise to substitutional doping, as confirmed by XPS analysis. The replacement of some Ti^{4+} by Cu^+ introduces more defects; in particular, the generation of oxygen vacancies due to the charge compensation effect implies that the tetragonal anatase structure is perturbed: each of the three Ti atoms near the vacancy moves away towards their five remaining oxygen neighbors. As a consequence, the Ti-O bond length is shortened and the resulting bonding energy is increased.[32] It is also worth noting that the doped films exhibited higher N_D compared to undoped TiO_2 due to a larger concentration of donor states, most likely attributable to oxygen vacancies states with one or two electrons, which act as shallow donors and are generated due to the deficiency of an oxygen atom in the bulk or on the surface.[33] But while the larger doping density improved the charge transport and transfer efficiency, resulting in a higher photocurrent density in N-TiO_2, it did not have the same beneficial effect on the photoectrochemical performance of Cu-TiO_2. In this case, the increased doping density induced a larger number of recombination centers and trap states. Therefore it can be reasonably inferred that the generation of multiple defective sites due to the doping affects significantly the electrochemical behavior: on the one hand, as in the case of N-TiO_2, the presence of defects it is evident and it can likely be associated with oxygen vacancies,

which are particularly beneficial for the separation of charge carriers and the transfer of the latter ones through the solid/electrolyte interface; on the other hand, doping translates into defects being detrimental to the photoelectrochemical performance. This is the case of Cu-doped in TiO_2, where atomic rearrangements and surface reconstruction triggered by the incorporation Cu^+ into anatase structure resulted in charge carriers recombination centers. These recombination centers can be ascribed both to Cu^+ entities themselves and probably to adverse trap states attributable to the excessive charge unbalance within the Cu-TiO_2 lattice.

Table 1. R_1, R_2 and CPE_2 obtained from equivalent circuit under UV/Vis irradiation, E_{FB}, N_D, SCA and F_{AD} before and after UV/Vis irradiation.

Sample	R_1 (Ω cm^{-2})	R_2 (Ω cm^{-2})	CPE_2 (μF cm^{-2})	E_{FB} (V)	N_D x 10^{18} (cm^{-3})	SCA (°)		F_{AD} (nN)	
						Before UV/Vis	After UV/Vis	Before UV/Vis	After UV/Vis
TiO_2	99.4	1049	8.3	- 0.189	6.8	48	10	0.77	1.19
Cu-TiO_2	107.6	1192	10.4	- 0.172	9.0	18	<5	1.43	1.62
N-TiO_2	40.8	641	7.1	- 0.148	12.4	10	<5	1.02	1.24

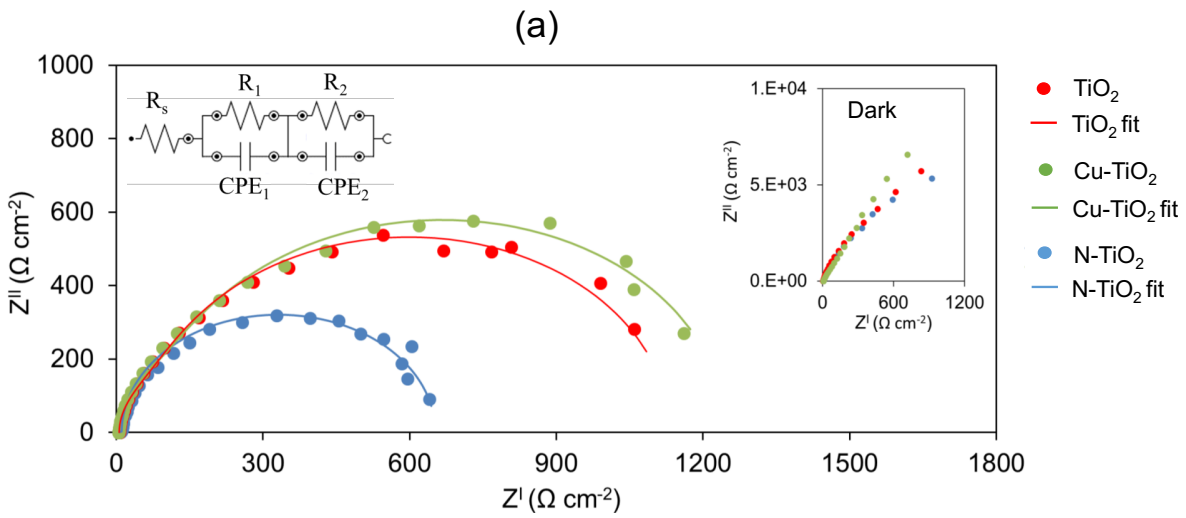

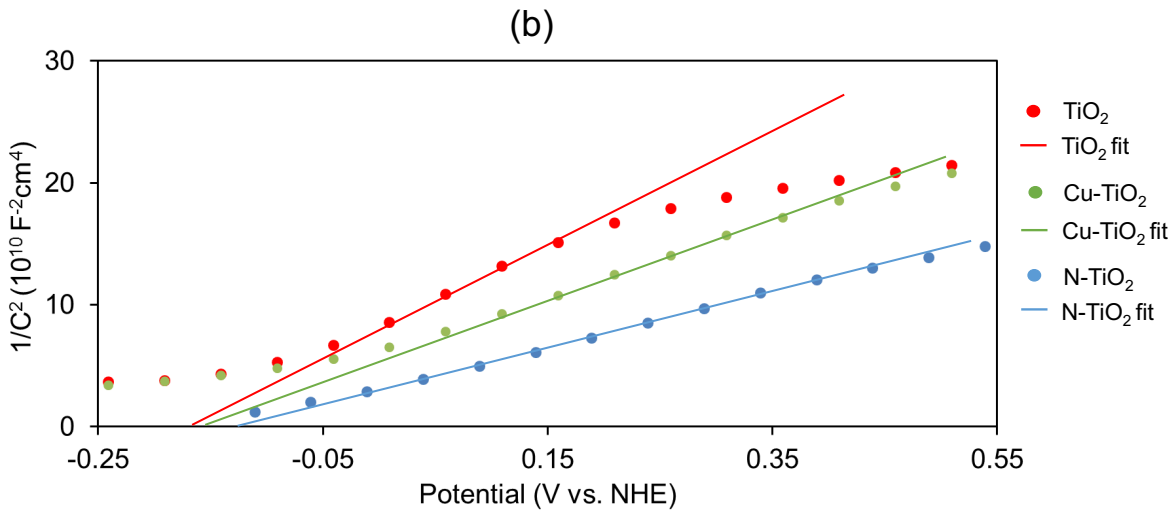

Figure 2. **(a)** Nyquist plots of EIS measurements of the three thin films obtained under UV/Vis irradiation. Equivalent fitting circuit and Nyquist plot under dark conditions are showed in the insets. Data are obtained at 0.9 V vs.NHE **(b)** Mott-Schottky plots of the three thin films.

The assessment of wettability was achieved macroscopically through an investigation carried out by SCA measurements, the results of which are illustrated in Fig. 3. Before UV/Vis exposure, pure TiO_2 film was the most hydrophobic with SCA = 48 ± 6°, whereas doped films were much more hydrophilic with SCA of 18 ± 5° for Cu-TiO_2 and 10 ± 3° for N-TiO_2, giving evidence of the positive effect of both types of doping on the film wettability. The enhanced hydrophilicity of the doped materials can be ascribed to a larger number of oxygen vacancies as compared to pristine TiO_2. A large density of oxygen vacancies infers that, when water droplet stands on the film surface, water molecules tend to occupy oxygen vacancies producing a large amount of adsorbed OH groups, which make the film surface more hydrophilic.[34-35] Unlike the photoelectrochemical characterization, Cu-TiO_2 performs better than bare TiO_2. This suggests that oxygen vacancies plays a major role here than others defects unfavorable for the photoelectrochemical performance. After 30 min exposure time to UV/Vis light, the SCA decreased to 10 ± 2° for pure TiO_2, while doped materials were found to be superhydrophilic with water droplet spreading completely and evenly upon the film surface. The exposure to UV/Vis light indeed induces a large amount of defective sites which boost film hydrophilicity: the reaction of the holes with lattice oxygen results in the formation of further oxygen vacancies sites into which more water molecules can coordinate; whereas some of the electrons react with lattice Ti^{4+} to form Ti^{3+}, which tends to react immediately with oxygen molecules adsorbed on the surface.[36]

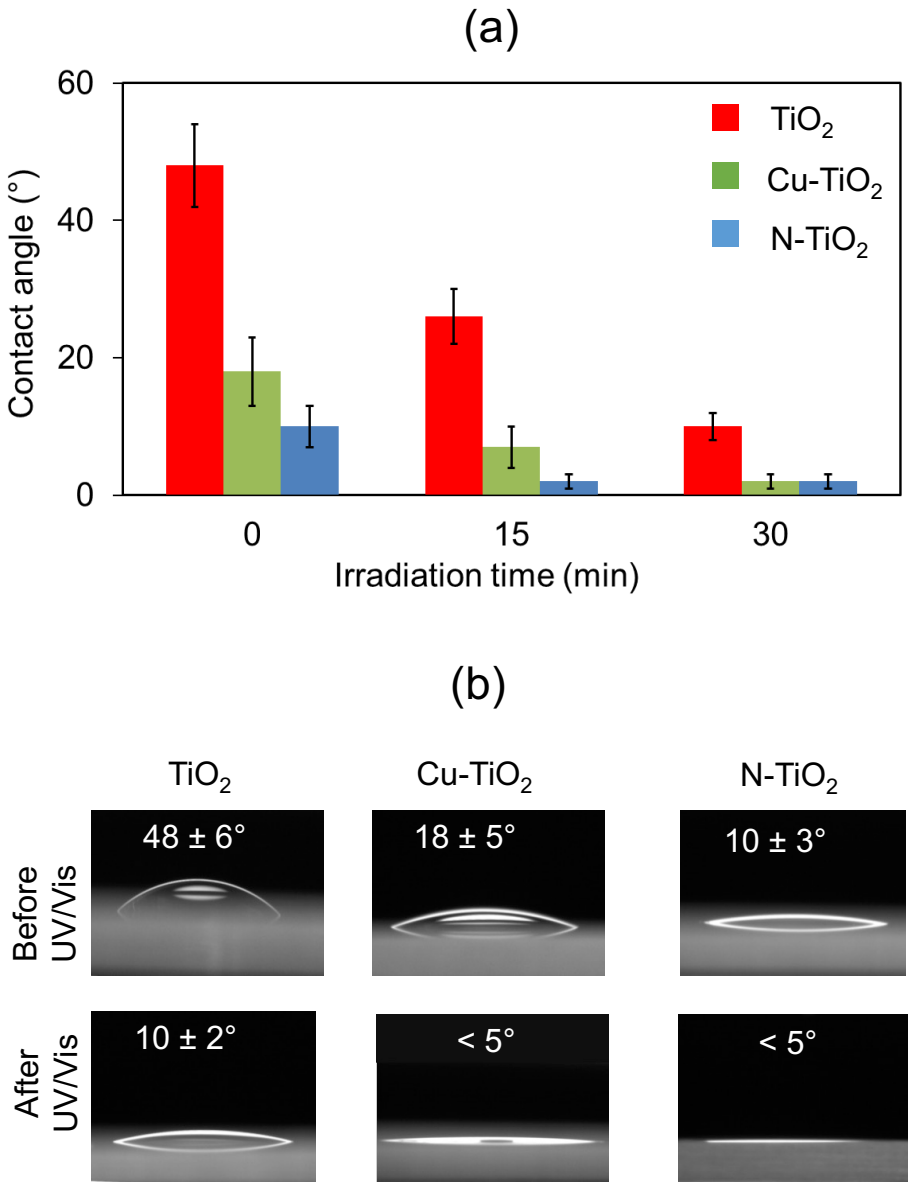

Figure 3. (a) Time evolution under UV/Vis irradiation of the SCA for TiO_2, Cu-TiO_2, and N-TiO_2. **(b)** Water drop images of the three samples at t = 0 min and after 30 min.

The macroscopic investigation results were in agreement with nanoscopic measurements using AFM based force spectroscopy. As shown in Fig. 4a, we have reconstructed the force profiles between an AFM probe and the samples, *i.e.* TiO_2, Cu-TiO_2, and N-TiO_2. The minimum value in the force profile is defined as adhesion force (F_{AD}). For clarity sake, we take the absolute value of F_{AD} and the results are presented in Fig. 4b. By invoking the sphere-plane model, we obtain the relationship between F_{AD} and surface energy: [37-38]

$$F_{AD} = 4\pi R\gamma \quad (4)$$

where, R is the AFM probe radius which is constantly monitored *in situ* with the critical amplitude method[19] to ensure that there was no change in R while probing TiO_2, Cu-TiO_2, and N-TiO_2. As we carefully kept R constant, we could deduce that F_{AD} is directly proportional to the surface energy γ. We can see from Fig. 4b that N-TiO_2 has the highest F_{AD} while TiO_2 has the lowest value, which implied that N-TiO_2 has the highest surface energy and TiO_2 the lowest. The respective F_{AD} value for TiO_2, Cu-TiO_2, and N-TiO_2 reads 0.58 ± 0.25 nN, 0.64 ± 0.17 nN, and 0.74 ± 0.18 nN. This is in agreement with SCA measurements showing that N-TiO_2 presented lowest SCA and TiO_2 the highest.

The surface energy of any surface is related to the extent of spontaneous interaction with liquid or vapor and completely depends on its surface characteristics[13, 39] (i.e., surface topography, chemical composition, roughness). We have measured the surface root mean square roughness of TiO_2, Cu-TiO_2, and N-TiO_2, which reads 3.8 nm, 3.4 nm, and 3.2 nm, respectively. The similar roughness and morphology of the three films (Fig. S2) suggest that the decisive factor here is the chemical composition. As in the case of photoelectrochemical properties, the different hydrophilicity of the three films is therefore due to the doping and its effect on the surface chemistry. Therefore, it can be reasonably proposed that the rise in hydrophilic character in doped films is linked to the progressive increase in surface oxygen vacancies following the Cu and N doping, given that the wettability properties are only produced by a chemical surface modification. AFM measurements are thus in line with this hypothesis: the larger surface energy and F_{AD} in doped samples result from a greater number of oxygen vacancies acting as binding sites for ambient water molecules, with a consequent enhanced water coverage of the film surface. Interestingly, opto-electronic and wettability properties are consistent with each other: the gradual increase in N_D and positive shift of E_{FB} observed in C-V measurements, when switching from pure TiO_2 to Cu-TiO_2 and N-TiO_2, follows the trend of SCA and AFM data. The improvement in wettability, indeed, occurs together with an increasing concentration of inter-bandgap donor states (i.e. oxygen vacancies) accounted for N_D and a positive shit of E_{FB} (Table 1).

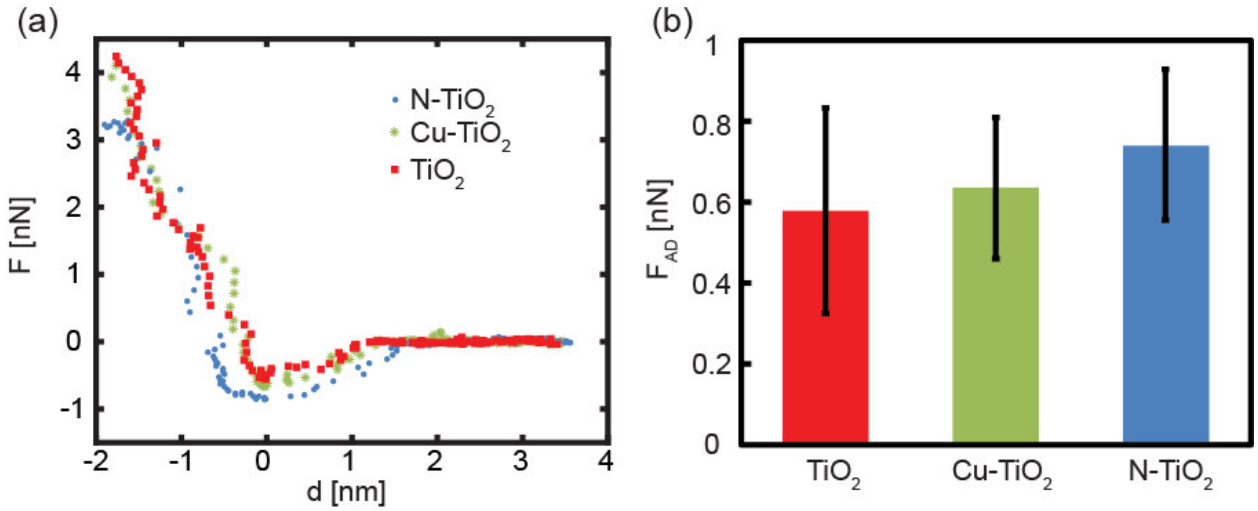

Figure 4. (a) Representative force profiles reconstructed from AFM force spectroscopy for TiO_2, Cu-TiO_2, and N-TiO_2 before UV/Vis irradiation. **(b)** F_{AD} values extracted from force profiles.

The effect of UV/Vis irradiation on TiO_2, Cu-TiO_2, and N-TiO_2 samples was also evaluated by AFM force spectroscopy. We first recorded APD curves of the sample and, then, let the sample exposed to UV/Vis irradiation, before retaking APD curves with the identical AFM probe for each sample. As shown in Fig. 5, we can see a consistent increase trend of F_{AD} after UV/Vis irradiation for all of the samples (TiO_2, Cu-TiO_2, and N-TiO_2). This quantifies the change in surface properties due to the effect of UV/Vis radiation. The histogram in Fig. 5 represents the average F_{AD} collected from thousands of curves before and after illumination. The absolute values for the F_{AD} are comparable between each sample where extreme care was taken to avoid tip damage and or contamination. On the other hand, the F_{AD} values are not comparable across the samples TiO_2, Cu-TiO_2, and N-TiO_2 of Fig. 5 since different tips were employed. However, as we can see in Fig. 5, the increase of TiO_2 F_{AD} after UV/Vis irradiation is clearly larger than other Cu-TiO_2 and N-TiO_2 samples. That is, the F_{AD} of TiO_2 increased from 0.77 ± 0.25 nN to 1.19 ± 0.64 nN. This is also in line with macroscopic SCA measurement results as the contact angle of TiO_2 decreased from $48 \pm 6°$ to $10 \pm 2°$.

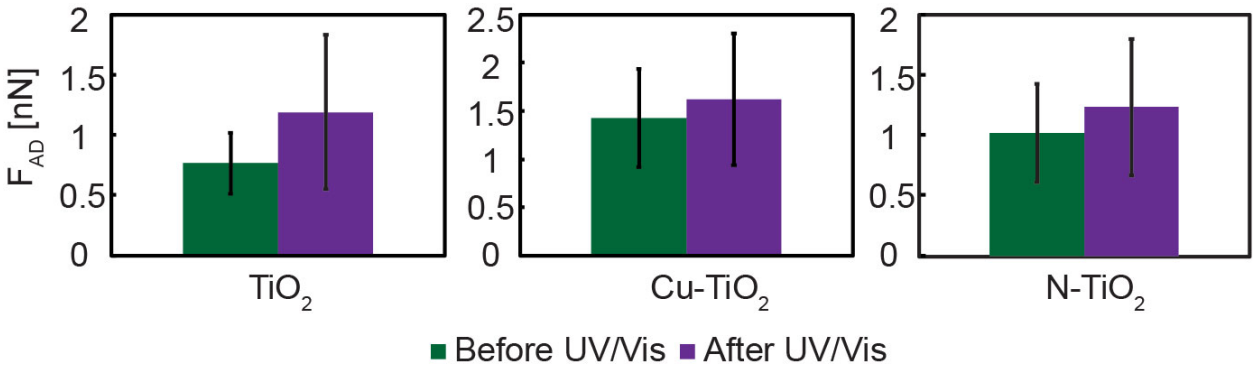

Figure 5. F_{AD} against TiO_2, Cu-TiO_2, and N-TiO_2 for before and after 30 min of UV/Vis irradiation.

4. Conclusions

In the present study, the electrochemical behavior and surface wettability of pure, N-doped and Cu-doped TiO_2 films were investigated before and after exposure to UV irradiation. Photoelectrochemical characterization showed that Cu doping did not improve the photoconversion efficiency due to the tendency of Cu(I) to act as charge carrier trap, where e–h recombination occurs. On the other hand, nitrogen doping enhanced the photoresponse due to the improved separation efficiency of photoinduced carriers as corroborated by best anodic photocurrent response and as well as electrochemical impedance spectroscopy, which pointed out a faster charge transfer at the film-liquid interface in N-TiO_2 thin films (i.e. $R_2 \approx 650\ \Omega\ cm^{-2}$ lower than $R_2 \approx 1050$ and $1200\ \Omega\ cm^{-2}$ exhibited by TiO_2 and Cu-TiO_2, respectively). The anodic shift of flat band potential and increase in doping density in Cu-TiO_2 and, more sharply, in N-TiO_2 were matched by a significant improvement in film hydrophilicity associated with the occurrence of more surface defects, such as oxygen vacancies, which serve as binding sites for water molecules. These alterations in surface chemistry were supported by nanoscale investigation through AFM, which revealed an increase in the adhesion force F_{AD} following UV exposure, indicating therefore a higher surface energy responsible for enhanced wetting of the surface. The nanoscopic observation by AFM was consistent with macroscopic wettability measurements: N-TiO_2 was the most hydrophilic sample in the dark (contact angle ~ 10°) and became superhydrophilic, as well as Cu-TiO_2, after UV irradiation, giving further evidence that both types of doping are effective routes for boosting the hydrophilicity.

The present work provides evidence that photoelectrochemical properties and wettability of TiO_2 films can be related to each other based on a common denominator, namely the surface chemistry. The importance of the present study also lies in the fact that it reveals the possibility of extending

the proposed approach from TiO_2 to other oxide semiconductors such as ZnO and WO_3, which is certainly significant for further improving the performance of such materials in a plethora of applications including for example multipurpose self-cleaning coatings and photoelectrodes in PEC.

Acknowledgements

C.G. and G.P. would like to thank Masdar Institute of Science and Technology (now part of Khalifa University of Science and Technology) for financial support (Grant No. SSG2017-000007).

Additional information

Supplementary information with XRD and AFM topography is available for this paper.

References

(1) Torralvo, M.; Sanz, J.; Sobrados, I.; Soria, J.; Garlisi, C.; Palmisano, G.; Çetinkaya, S.; Yurdakal, S.; Augugliaro, V. Anatase Photocatalyst with Supported Low Crystalline TiO_2: The Influence of Amorphous Phase on the Activity. *Appl. Catal., B* **2018**, *221*, 140-151.

(2) Yang, Y.; Zhang, T.; Le, L.; Ruan, X.; Fang, P.; Pan, C.; Xiong, R.; Shi, J.; Wei, J. Quick and Facile Preparation of Visible Light-Driven TiO_2 Photocatalyst with High Absorption and Photocatalytic Activity. *Sci. Rep.* **2014**, *4*, 7045.

(3) Li, X.; He, J. Synthesis of Raspberry-Like SiO_2–TiO_2 Nanoparticles toward Antireflective and Self-Cleaning Coatings. *ACS Appl. Mater. Interfaces* **2013**, *5*, 5282-5290.

(4) Yaghoubi, H.; Taghavinia, N.; Alamdari, E. K. Self Cleaning TiO_2 Coating on Polycarbonate: Surface Treatment, Photocatalytic and Nanomechanical Properties. *Surf. Coat. Technol.* **2010**, *204*, 1562-1568.

(5) Wang, Y.; Zhang, Y.-Y.; Tang, J.; Wu, H.; Xu, M.; Peng, Z.; Gong, X.-G.; Zheng, G. Simultaneous Etching and Doping of TiO_2 Nanowire Arrays for Enhanced Photoelectrochemical Performance. *ACS Nano* **2013**, *7*, 9375-9383.

(6) Sun, L.; Cai, J.; Wu, Q.; Huang, P.; Su, Y.; Lin, C. N-Doped TiO_2 Nanotube Array Photoelectrode for Visible-Light-Induced Photoelectrochemical and Photoelectrocatalytic Activities. *Electrochim. Acta* **2013**, *108*, 525-531.

(7) Fan, J.; Li, Z.; Zhou, W.; Miao, Y.; Zhang, Y.; Hu, J.; Shao, G. Dye-Sensitized Solar Cells Based on TiO_2 Nanoparticles/Nanobelts Double-Layered Film with Improved Photovoltaic Performance. *Appl. Surf. Sci.* **2014**, *319*, 75-82.

(8) Takeuchi, M.; Sakamoto, K.; Martra, G.; Coluccia, S.; Anpo, M., Mechanism of Photoinduced Superhydrophilicity on the TiO_2 Photocatalyst Surface. *J. Phys. Chem. B* **2005**, *109*, 15422-15428.

(9) Yang, G.; Jiang, Z.; Shi, H.; Xiao, T.; Yan, Z. Preparation of Highly Visible-Light Active N-Doped TiO_2 Photocatalyst. *J. Mater. Chem.* **2010**, *20*, 5301-5309.

(10) Karunakaran, C.; Abiramasundari, G.; Gomathisankar, P.; Manikandan, G.; Anandi, V. Cu-Doped TiO_2 Nanoparticles for Photocatalytic Disinfection of Bacteria under Visible Light. *J. Colloid Interface Sci.* **2010**, *352*, 68-74.

(11) Garlisi, C.; Scandura, G.; Szlachetko, J.; Ahmadi, S.; Sa, J.; Palmisano, G., E-Beam Evaporated TiO_2 and Cu-TiO_2 on Glass: Performance in the Discoloration of Methylene Blue and 2-Propanol Oxidation. *Appl. Catal., A* **2016**, *526*, 191-199.
(12) Radecka, M.; Rekas, M.; Trenczek-Zajac, A.; Zakrzewska, K. Importance of the Band Gap Energy and Flat Band Potential for Application of Modified TiO_2 Photoanodes in Water Photolysis. *J. Power Sources* **2008**, *181*, 46-55.
(13) Garlisi, C.; Scandura, G.; Palmisano, G.; Chiesa, M.; Lai, C.-Y. Integrated Nano- and Macroscale Investigation of Photoinduced Hydrophilicity in TiO_2 Thin Films. *Langmuir* **2016**, *32*, 11813-11818.
(14) Kang, Q.; Cao, J.; Zhang, Y.; Liu, L.; Xu, H.; Ye, J. Reduced TiO_2 Nanotube Arrays for Photoelectrochemical Water Splitting. *J. Mater. Chem. A* **2013**, *1*, 5766-5774.
(15) Katan, A. J.; van Es, M. H.; Oosterkamp, T. H. Quantitative Force Versus Distance Measurements in Amplitude Modulation Afm: A Novel Force Inversion Technique. *Nanotechnology* **2009**, *20*, 165703.
(16) Sader, J. E.; Jarvis, S. P. Accurate Formulas for Interaction Force and Energy in Frequency Modulation Force Spectroscopy. *Appl. Phys. Lett.* **2004**, *84*, 1801-1803.
(17) Amadei, C. A.; Santos, S.; Pehkonen, S. O.; Verdaguer, A.; Chiesa, M. Minimal Invasiveness and Spectroscopy-Like Footprints for the Characterization of Heterogeneous Nanoscale Wetting in Ambient Conditions. *J. Phys. Chem. C* **2013**, *117*, 20819-20825.
(18) Plummer, A.; Tang, T.-C.; Lai, C.-Y.; Chiesa, M. Nanoscale Hydrophilicity Studies of Gulf Parrotfish (Scarus Persicus) Scales. *ACS Appl. Mater. Interfaces* **2014**, *6*, 16320-16326.
(19) Santos, S.; Guang, L.; Souier, T.; Gadelrab, K.; Chiesa, M.; Thomson, N. H. A Method to Provide Rapid in Situ Determination of Tip Radius in Dynamic Atomic Force Microscopy. *Rev. Sci. Instrum.* **2012**, *83*, 043707.
(20) Sun, B.; Shi, T.; Peng, Z.; Sheng, W.; Jiang, T.; Liao, G. Controlled Fabrication of Sn/TiO_2 Nanorods for Photoelectrochemical Water Splitting. *Nanoscale Res. Lett.* **2013**, *8*, 462.
(21) Aragaw, B. A.; Pan, C.-J.; Su, W.-N.; Chen, H.-M.; Rick, J.; Hwang, B.-J. Facile One-Pot Controlled Synthesis of Sn and C Codoped Single Crystal TiO_2 Nanowire Arrays for Highly Efficient Photoelectrochemical Water Splitting. *Appl. Catal., B* **2015**, *163*, 478-486.
(22) Zhang, N.; Yang, M.-Q.; Liu, S.; Sun, Y.; Xu, Y.-J. Waltzing with the Versatile Platform of Graphene to Synthesize Composite Photocatalysts. *Chem. Rev.* **2015**, *115*, 10307-10377.
(23) Yang, M.-Q.; Xu, Y.-J. Selective Photoredox Using Graphene-Based Composite Photocatalysts. *Phys. Chem. Chem. Phys.* **2013**, *15*, 19102-19118.
(24) Lopes, T.; Andrade, L.; Le Formal, F.; Gratzel, M.; Sivula, K.; Mendes, A. Hematite Photoelectrodes for Water Splitting: Evaluation of the Role of Film Thickness by Impedance Spectroscopy. *Phys. Chem. Chem. Phys.* **2014**, *16*, 16515-16523.
(25) Wang, S.; Zhang, J.; Chen, S.; Yang, H.; Lin, Y.; Xiao, X.; Zhou, X.; Li, X. Conversion Enhancement of Flexible Dye-Sensitized Solar Cells Based on TiO_2 Nanotube Arrays with TiO_2 Nanoparticles by Electrophoretic Deposition. *Electrochim. Acta* **2011**, *56*, 6184-6188.
(26) Duan, Y.; Fu, N.; Liu, Q.; Fang, Y.; Zhou, X.; Zhang, J.; Lin, Y. Sn-Doped TiO_2 Photoanode for Dye-Sensitized Solar Cells. *J. Phys. Chem. C* **2012**, *116*, 8888-8893.
(27) Beranek, R. (Photo)Electrochemical Methods for the Determination of the Band Edge Positions of TiO_2-Based Nanomaterials. *Adv. Chem. Phys* **2011**, *2011*, 20.
(28) Garlisi, C.; Szlachetko, J.; Aubry, C.; Fernandes, D. L. A.; Hattori, Y.; Paun, C.; Pavliuk, M. V.; Rajput, N. S.; Lewin, E.; Sá, J.; Palmisano, G. N-TiO_2/Cu-TiO_2 Double-Layer Films: Impact of Stacking Order on Photocatalytic Properties. *J. Catal.* **2017**, *353*, 116-122.
(29) Premkumar, J. Development of Super-Hydrophilicity on Nitrogen-Doped TiO_2 Thin Film Surface by Photoelectrochemical Method under Visible Light. *Chem. Mater.* **2004**, *16*, 3980-3981.
(30) Irie, H.; Washizuka, S.; Watanabe, Y.; Kako, T.; Hashimoto, K. Photoinduced Hydrophilic and Electrochemical Properties of Nitrogen-Doped TiO_2 Films. *J. Electrochem. Soc.* **2005**, *152*, E351-E356.

(31) Yang, G.; Jiang, Z.; Shi, H.; Xiao, T.; Yan, Z. Preparation of Highly Visible-Light Active N-Doped TiO_2 Photocatalyst. *J. Mater. Chem.* **2010**, *20*, 5301-5309.
(32) Wang, S.; Meng, K.; Zhao, L.; Jiang, Q.; Lian, J. Superhydrophilic Cu-Doped TiO_2 Thin Film for Solar-Driven Photocatalysis. *Ceram. Int.* **2014**, *40*, 5107-5110.
(33) Boonchun, A.; Reunchan, P.; Umezawa, N. Energetics of Native Defects in Anatase TiO_2: A Hybrid Density Functional Study. *Phys. Chem. Chem. Phys.* **2016**, *18*, 30040-30046.
(34) Park, J.-J.; Kim, D.-Y.; Latthe, S. S.; Lee, J.-G.; Swihart, M. T.; Yoon, S. S. Thermally Induced Superhydrophilicity in TiO_2 Films Prepared by Supersonic Aerosol Deposition. *ACS Appl. Mater. Interfaces* **2013**, *5*, 6155-6160.
(35) Garlisi, C.; Palmisano, G. Radiation-Free Superhydrophilic and Antifogging Properties of E-Beam Evaporated TiO_2 Films on Glass. *Appl Surf Sci* **2017**, *420*, 83-93.
(36) Sun, R.-D.; Nakajima, A.; Fujishima, A.; Watanabe, T.; Hashimoto, K. Photoinduced Surface Wettability Conversion of ZnO and TiO_2 Thin Films. *J. Phys. Chem. B* **2001**, *105*, 1984-1990.
(37) Yaminsky, V. V. The Hydrophobic Force: The Constant Volume Capillary Approximation. *Colloids Surf. Physicochem. Eng. Aspects* **1999**, *159*, 181-195.
(38) Israelachvili, J. *Intermolecular & Surface Forces*, 2 ed.; Academic Press: New York, 1991.
(39) Lai, C.-Y.; Cozzolino, M.; Diamanti, M. V.; Al Hassan, S.; Chiesa, M., Underlying Mechanism of Time Dependent Surface Properties of Calcite ($CaCO_3$): A Baseline for Investigations of Reservoirs Wettability. *J. Phys. Chem. C* **2015**, *119*, 29038-29043.